이학석사 학위논문

$BRAF^{V600E}$ Transduction of SV40-immortalized Normal Human Thyroid Cells Induces Dedifferentiated Thyroid Carcinogenesis in a Mouse Xenograft Model

$BRAF^{V600E}$ 돌연변이가 SV40-형질도입 인간 정상 갑상선 세포주의 마우스 이종이식 모델에서 갑상선암의 역분화에 미치는 영향 연구

2019년 02월

서울대학교 대학원

협동과정 종양생물학 전공

김 민 준

$BRAF^{V600E}$ 돌연변이가 SV40-형질도입 인간 정상 갑상선 세포주의 마우스 이종이식 모델에서 갑상선암의 역분화에 미치는 영향 연구

지도교수 김 수 진

이 논문을 이학석사 학위논문으로 제출함

2018년 10월

서울대학교 대학원

협동과정 종양생물학 전공

김 민 준

김 민 준의 석사 학위논문을 인준함

2019년 01월

위 원 장 _____ (인)

부 위 원 장 _____ (인)

위 원 _____ (인)

$BRAF^{V600E}$ Transduction of SV40-immortalized Normal Human Thyroid Cells Induces Dedifferentiated Thyroid Carcinogenesis in a Mouse Xenograft Model

by

Minjun Kim

A thesis submitted to the Interdisciplinary Graduate Program in partial fulfillment of the requirements for the Degree of Master of Philosophy in Cancer Biology at Seoul National University Graduate School

January 2018

Approved by Thesis Committe:

Professor _____ Chairman

Professor _____ Vice chairman

Professor _____

Abstract

Introduction: $BRAF^{V600E}$ is the most common mutation in thyroid carcinomas. Although its clinical importance has been actively studied, a proper research model to investigate the role of $BRAF^{V600E}$ in etiopathogenesis of human thyroid cancers has not been established. Thus, we xenografted the two stable cell lines Nthy/$BRAF^{WT}$ (Nthy/WT) and Nthy/$BRAF^{V600E}$ (Nthy/V600E), which are SV40-immortalized normal human thyroid cell line Nthy-ori 3-1 (Nthy) expressing $BRAF^{WT}$ or $BRAF^{V600E}$ by lentiviral transduction to study the role of $BRAF^{V600E}$ in human thyroid carcinogenesis and establish a new in vivo research model for human thyroid cancer with $BRAF^{V600E}$.

Methods: Nthy/WT and Nthy/V600E were subcutaneously injected into NSG mice. Hematoxylin and Eosin stain and immunohistochemical analysis were performed for a pathological analysis. $BRAF^{V600E}$-selective inhibitor (vemurafenib) was treated to confirm $BRAF^{V600E}$-induced tumorigenesis and metastasis. Transcriptomic changes were analyzed using RNA-sequencing, and a comparative transcriptome analysis was performed based on data from The Cancer Cell Line Encyclopedia and Gene Expression Omnibus (GSE33630).

Results: While Nthy/WT did show neither in vivo tumorigenesis nor metastasis, Nthy/V600E formed tumors reaching 2784.343 ± 922.463 mm3 (mean ± standard deviation, n = 11) and metastasized to the relevant lymph nodes in 72.7% (8/11) in 4 weeks and to the lung and liver in 6 to 7 weeks. Vemurafenib treatment significantly inhibited the tumor growth and metastasis, but it could not induce an apoptosis. In a pathological analysis, Nthy/V600E closely corresponded to dedifferentiated thyroid cancer. A comparative transcriptomic analysis revealed that 5512 DEGs (|FC| ≥ 2, adjusted p < 0.01) between Nthy/WT and Nthy/V600E are shared more with ATC than PTC tissues. Also, gene expression patterns associated with differentiation and cancer prognosis were very similar with human ATC cell line 8305c. $BRAF^{V600E}$ activated a cell cycle of a contact-inhibited Nthy by up- and down-regulating genes involved in G1 progression and G1/S arrest, respectively.

Conclusion: Our data show that $BRAF^{V600E}$ plays a pivotal role in carcinogenesis of SV40-transfected normal human thyroid cells, and it also suggests that SV40 might contribute to dedifferentiated thyroid carcinogenesis in this model. A xenograft model of the cell lines would be a new model to study etiopathogenesis and possible

therapies of dedifferentiated thyroid cancer.

Keywords: Thyroid carcinogenesis, BRAF V600E, simian virus 40, dedifferentiated thyroid cancer, RNA-sequencing, mouse xenograft model, vemurafenib

Student number: 2017-22690

Contents

List of Tables

List of Figures

Introduction

Chapter 1. Thyroid cancer

Epidemiological backgrounds of thyroid cancer

According to the reports from National Cancer Institute (NIH, USA) and Cancer Research UK (UK), the incidence of thyroid carcinomas has been increasing over the past 10 years. Especially, South Korea had a dramatic increase in the incidence of thyroid carcinomas and it provoked many issues on over-diagnosis(8). Thyroid cancer, however, is still most prevalent and the incidence is still high recording the third incidence among all cancers in 2015 despite doubts casted by the controversy (National Cancer Information Center, Korea).

Traditional classification of thyroid cancers

Thyroid neoplasms are defined mainly based on their pathologic signatures and classified into five types: differentiated types such as papillary thyroid cancer (PTC) and folicullar thyroid cancer (FTC), advanced types such as medullary thyroid cancer (MTC), poorly differentiated thyroid cancer (PDTC), and anaplastic

thyroid cancer (ATC). Each type of thyroid cancers shows different clinicopathological features.

Differentiated thyroid carcinomas: PTC and FTC

PTC is the most common type consisting of about 75 – 85% of all thyroid cancer cases(9). It is originated from thyroid follicular epithelial cells and shows well-differentiated and favorable clinical outcomes showing only locoregional metastasis to the relevant lymph nodes such as cervical lymph nodes in most cases, showing over 90% 5-year survival rate in most countries(9). Especially, one of the variant of PTC, follicular variant papillary thyroid cancer (fvPTC) is now considered as a benign tumor if it shows an encapsulated histological phenotype, reclassified as the noninvasive follicular thyroid neoplasm with papillary-like nuclear features (NIFTP)(10).

FTC is found in about 10 – 15% of all cases(11). Like PTC, it is also follicular-originated and well-differentiated, but more aggressive than PTC(12). They tend to metastasize hematogenously into other organs such as the lung and bone(12). While overall 5-year survival is over 90% like PTC, it is markedly different depending on the stages of cancer(13). Especially, Hurthle cell cancer, which is a variant of FTC, is usually more

aggressive(14).

Advanced thyroid carcinomas: MTC, PDTC, and ATC

Unlike other thyroid cancers, MTC originates from the parafollicular C-cells and is known to exist as both familial and sporadic form, accounting for approximately 3% of all cases(15). Clinical outcome is relatively worse than PTC and FTC showing about 83% of 5-year survival rate(16).

PDTC and ATC are considered as more advanced types from the differentiated ones such as PTC and FTC(17). They both are very aggressive and resistant to many of the currently available therapies including small-molecule drugs and radioactive iodine therapy(17). Because of those characteristics, their clinical outcomes are very poor.

PDTC is an intermediate form between differentiated thyroid carcinomas and anaplastic thyroid carcinoma when it comes to clinicopathological features as well as differentiation status, sometimes confusing pathologists and clinicians(17, 18).

ATC has a very poor prognosis including a distant metastasis and frequent recurrence, resulting in almost 100% of disease-specific mortality(19). ATC is diagnosed based on clinical and pathologic features(19). According to The Papanicolaou Society of

Cytopathology Consensus Recommendations, in clinical features, ATC grows rapidly and is found with several metastases at the initial diagnosis(19). Also, cytologic features of ATC include highly malignant cells in a combination of spindle, giant, and squamoid cells with high-grade nuclear features such as marked pleomorphism, dark clumped chromatin, macronucleoli, and atypical mitoses. On top of that, it rarely expresses Tg and TTF-1 while PAX8 expression is usually maintained(20). Even though the Food and Drug Administration (FDA, USA) recently approved a combinatorial therapy using dabrafenib and trametinib for $BRAF^{V600E}$-positive ATC, it is still impossible to completely treat ATC as of now(21).

Molecular classification of thyroid cancers

Thyroid cancers have long been classified as histological subtypes, but a new paradigm for classification of thyroid cancers is arising. There are several oncogenic genetic alterations that are very prevalent and common in well-differentiated thyroid cancers; $BRAF^{V600E}$, *RAS* gene family (*H/K/NRAS*), *RET, RET/PTC* rearrangements, *PAX8-peroxisome proliferator-activated receptor* γ (*PPARγ*) fusion gene. These mutations are usually mutually exclusive and found with a few to many other pathogenic alterations(9).

BRAF^{V600E}, which is the most common mutation in thyroid carcinomas, is found in about 45.7% of all cases and in 48.5% – 80.8% of PTC followed by *RAS* family mutations and RET/PTC rearrangements(22–24). The frequencies vary depending on the subtype of PTC. For example, BRAF^{V600E} was found in 71.43% of classical PTC and 25% of fvPTC while H/K/N Ras mutations found in 1.3% of classical PTC and 47.92% of fvPTC(25).

Unlike PTC, H/K/NRAS mutations are most commonly found in FTC while BRAF^{V600E} is found in no or only few cases. PAX8–PPARγ fusion is also often expressed in FTC(26). Recent studies based on next–generation sequencing revealed that these mutations are closely associated with a specific histological type and a distinct pattern of gene expressions as well as clinical outcomes, suggesting a new classification of differentiated thyroid cancers; BRAF–like, RAS–like, and Non–BRAF Non–RAS (NBNR) subtypes(9, 25) depending on the driver genomic alterations.

Progression to anaplastic thyroid cancer

Progression of differentiated thyroid cancer is known to be associated with an accumulation of mutations on top of the driver alterations(27). Especially, genomic alterations in *TP53*, *TERT* promoter, and *PI3K–AKT* pathways have been reported as a key

contributor to a poor prognosis and progression to advanced thyroid carcinomas such as poorly differentiated thyroid cancer (PDTC) and ATC(27-31). For example, several studies reported that *TERT* promoter mutation is closely connected to thyroid cancer prognosis(28, 30, 32) and Pozdeyev et al. investigated molecular backgrounds of 779 advanced carcinomas, showing that genomic alterations in tumor suppressors such as *RB1* and *TP53* and cell-cycle genes like *CDKN2A* are closely associated with ATC(27).

Chapter 2. Necessity of research models for thyroid cancers

Human thyroid cancer cell lines

In order to find a non-surgical treatment for thyroid cancers, it is necessary to understand etiopathogenesis of the malignancies using proper research models, considering the high frequency of thyroid cancer and prevalence of $BRAF^{V600E}$ in thyroid cancers. To study thyroid cancers, numerous human thyroid cancer cell lines have been established from not only ATC, but also differentiated thyroid cancers such as PTC and FTC(33). However, most of the human thyroid cancer cell lines originates from tumors with aggressive behavior and complex mutation status, resulting in a lack of proper research models to elucidate etiopathogenesis of thyroid

cancers(33, 34). Even the newly established 6 PTC cell lines by Henderson et al. are also from aggressive cases and harbor *TERT* promoter mutation in addition to driver mutations such as *BRAF* and *RAS*. Only one cell line does not carry *TERT* promoter mutation, but it is not tumorigenic in a mouse xenograft model, meaning that it cannot be used to establish *in vivo* research model for preclinical investigation.

Mouse models for thyroid cancers

In this context, Charles et al. showed thyroid-specific expression of $BRAF^{V600E}$ induces murine papillary thyroid cancer in a genetically engineered mouse. Moreover, McFadden et al. proved that $BRAF^{V600E}$ causes murine papillary thyroid cancer and loss of function in p53 promotes anaplastic transformation in $BRAF^{V600E}$-expressing murine thyroid epithelial cells(29). As a result of the study, murine ATC cell line TBP-3743 by $BRAF^{V600E}$ and loss of p53 function was established, and Borre et al. utilized the murine cell line to make an *in vivo* research model(29, 35). However, since molecular mechanism might not be equal between human and a mouse, the origin of the cell line is likely to be an issue.

Normal human thyroid cell lines stably expressing either $BRAF^{WT}$ or $BRAF^{V600E}$

To study the role of $BRAF^{V600E}$ in human thyroid epithelial cells, our group previously developed the two cell lines Nthy/$BRAF^{WT}$ (Nthy/WT) and Nthy/$BRAF^{V600E}$ (Nthy/V600E), where two cell lines having the same genetic background differ only by the mutation status of BRAF by transducing a normal human thyroid cell line Nthy-ori 3-1 (Nthy) to express either $BRAF^{WT}$ or $BRAF^{V600E}$ gene(36). Expression of $BRAF^{V600E}$ induced EMT in both cell morphology and genetic expression, resulting in gene enrichment in cancer-related pathways and increased ability in migration, invasion, and anchorage-independent growth(36). However, whether it can be established as an *in vivo* research model has not been investigated yet.

Chapter 3. Simian virus 40 in cell immortalization and transformation

SV40 in host cells

Simian virus 40 (SV40) is a polyomavirus that has been widely used to immortalize primary cells to establish a cell line. Even though its carcinogenicity is controversial, the roles of SV40 in host cell transformation have been well defined(2, 37). SV40 expresses two SV40 large T antigen (SV40 T-ag) and SV40 small

T antigen are products in early viral infection of SV40 involved in viral genome replication and regulation of host cell cycle(2). While SV40 small T antigen cannot solely transform host cells, SV40 T-ag plays a pivotal role in the mechanism by mainly inhibiting pRb and p53(2).

SV40 and thyroid cancers

Even in thyroid cancers, presence of SV40 in thyroid cancer specimens is reported by three studies so far(38-40). Especially, Vivaldi et al. showed that SV40 and its T-ag expression were found more frequently in aggressive subtypes of thyroid tumors, also showing co-presence of SV40 in normal tissues near their malignant nodules(39). However, Nthy, which is a normal human thyrocyte immortalized by SV40 transfection without any known genomic alterations, was not tumorigenic in an immunodeficient nude mouse. Taken together, SV40 is able to transform normal human thyroid epithelial cells, but it could not solely induce carcinogenesis of human thyroid, suggesting the possibility of SV40 as a contributor to cancer progression.

Here, we aimed to establish a mouse xenograft model using Nthy/V600E to investigate whether *in vivo* tumorigenesis of a

normal human thyroid cell line can be initiated by $BRAF^{V600E}$ mutation and evaluate the Nthy/V600E-xenografted mouse model as a basic model to develop precision medicine for $BRAF^{V600E}$-initiated thyroid carcinomas(41).

Materials and Methods

Cell culture

Both Nthy/WT and Nthy/V600E were grown in RPMI 1640 supplemented with 10% FBS (Biowest), 2 mM GlutaMAX™ (Gibco), and 100 U/ml penicillin-streptomycin (Gibco) in a humidified atmosphere of 5% CO_2 at 37°C. 80%-confluent cells were used for xenografts. RNA for RNA-sequencing was extracted after 24-hour incubation in 100%-confluent condition, keeping the media fresh. Cell stocks with a same passage were used for each set of experiments. A Short Tandem Repeat (STR) analysis was performed by Korean Cell Line Bank (Seoul, South Korea) using AmpFLSTR™ identifiler™ PCR Amplification Kit (Applied Biosystems) and validated that all the cell lines have the same STR profile as Nthy-ori 3-1 cell line. The absence of mycoplasma in the cell lines was demonstrated by Korean Cell Line Bank using e-

Myco™ plus Mycoplasma PCR Detection Kit.

Animal experiments

All studies were performed under a protocol approved by an Institutional Animal Care and Use Committee at Seoul National University (SNU-171221-3-2), and mice were cared and maintained in accordance with the recommendations of Biomedical Center for Animal Resource Development at Seoul National University College of Medicine. Each cell line was harvested using TrypLE™ Express (Gibco) and re-suspended at 1E7 cells/ml in cold PBS and kept at 4 ℃. The re-suspended cell suspension (100 μl) was subcutaneously injected into the right flank of 6-8 weeks-old male NSG mice (NOD.Cg-PrkdcscidIl2rgtm1Wjl/SzJl, The Jackson laboratory). Tumors were measured with a caliper and the volume of the tumors was calculated by $Width^2$ x Length/2 (mm^3). All injections and tumor measurement were performed under isoflurane anesthesia to minimize stress. At the end-point of experiments, mice were euthanized using a CO_2 chamber, and an autopsy was conducted to collect the primary tumors and any distinguishable metastatic tumors in the lung, liver, lymph nodes, and other subcutaneous sites. The collected tumors were fixed in

10% neutral buffered formalin solution (Sigma) for 12-24h and paraffin-embedded. A part of the collected tumors was frozen in a deep freezer.

For drug treatment, Nthy/V600E-xenografted mice were incubated for 14 days without any treatment and treated either 10 mg/kg of PLX-4032 (vemurafenib, STEMCELL technologies) or vehicle intraperitoneally on a daily basis from day 14 to day 28. PLX-4032 was solubilized in 6% DMSO, 10% Tween 80 (Sigma), and 84% PBS (v/v) at 3 mg/ml, and it was freshly prepared every day before treatment.

Histology and immunohistochemistry

For histological analysis, the formalin-fixed paraffin-embedded (FFPE) tissues were sectioned at a thickness of about 4-5 μm, stained with hematoxylin and eosin (H&E) using Autostainer XL (Leica), and immunohistochemistry (IHC) analysis was performed with commercially available antibodies against BRAF V600E (clone VE1, ready-to-use, mouse monoclonal, Ventana), PAX8 (clone MRQ-50, 1:100, mouse monoclonal, Cell Marque), Ki-67 (clone MIB-1, 1:100, mouse monoclonal, DAKO), p53 (clone DO-7, mouse monoclonal, DAKO), TTF-1 (clone SP141, ready-

to-use, rabbit monoclonal, Ventana), thyroglobulin (A 0251, 1:30000, rabbit polyclonal, DAKO) by the department of pathology at Seoul National University Hospital. The results of H&E and IHC analysis were examined by a specialized pathologist at Seoul National University Hospital.

RNA sequencing

Three biological replicates were prepared for each cell line, which are cultured for 4-5 days keeping media fresh to put them under a contact inhibition. RNA was extracted using RNeasy Mini Kit (QIAGEN) and assessed for quantity and quality using 2100 Bioanalyzer (Agilent Technologies).

The sequencing libraries were prepared using TruSeq Stranded mRNA LT Sample Prep Kit (Illumina) following the manufacturer's recommendation and sequenced on a NovaSeq 6000 platform (Illumina) by Macrogen (South Korea). The sequenced paired-end reads were aligned to UCSC hg19 using HISAT2(42), and StringTie (43) was used for transcript assembly.

To confirm the presence of SV40 large T antigen expression, the sequenced reads were also aligned to SV40gp6

sequence (NC_001669.1).

Comparative analysis of transcriptome

To compare transcriptome of our cell lines with other established cell lines and human specimens, we utilized The Cancer Cell Line Encyclopedia (CCLE) database (Broad Institute, USA) and GEO database (GSE33630).

In CCLE database, we used RPKM data of 9 human thyroid cancer cell lines; 4 ATC (8305c, 8505c, BHT101, CAL62), 1 PDTC (BCPAP), 4 FTC (TT2609C02, FTC238, FTC133, ML1). In GSE33630, we downloaded cDNA microarray data of human frozen specimens; 11 of ATC, 48 of PTC, 23 of normal thyroid tissues.

Row z-score of median-centered log2 RPKM (FPKM) of our cell lines was analyzed together with RPKM of the 9 cell lines from CCLE to show gene expressions associated thyroid differentiation and prognosis-related genes such as epithelial-mesenchymal transition(EMT) and therapeutic targets for monoclonal antibody-based immunotherapies. For heatmap display, gene expressions were illustrated based on row z-score of median-centered log2 RPKM (FPKM), and thyroid differentiation

score (TDS) was calculated using the mean value of the row z-scores across 14 thyroid metabolism and function genes excluding PAX8, which is known to be usually conserved even in ATC.

Differentially expressed genes (DEG) between Nthy/WT and Nthy/V600E were compared to those of ATC-normal tissues and PTC-normal tissues to confirm that Nthy/V600E more corresponds to ATC than well-differentiated thyroid cancers. DESeq2 package was used to select the DEGs meeting the following criteria; 2-fold change or 4-fold change with adjusted p-value (Q-value) <0.01. Gene ontology of up- or down-DEGs was extracted based on DAVID Biological Processes at level 5 with a cut-off of adjusted p-value < 0.05.

Statistical analysis

All statistical analyses were performed using GraphPad PRISM version 8.0.0 (GraphPad Software, San Diego, CA, USA). Data are presented as mean ± standard deviation. The independent t-test, paired t-test, or Mann-Whitney test (n < 10) was used for comparison of continuous variables. Statistical significance was defined as two-sided p-values < 0.05.

Results

BRAF^{V600E} transduction initiates carcinogenesis of SV40-immortalized normal thyroid cells

To investigate the role of BRAF^{V600E} in carcinogenesis of human thyroid cells, we xenografted both Nthy/WT and Nthy/V600E into NSG mice. For each group, 11 male mice at age of 6-8 weeks were used, and 100 ul of the resuspended cells in DPBS at 10^7 cells/ml was subcutaneously injected into the right flank of the mice under an isoflurane anesthesia. As a result, Nthy/V600E formed a distinguishable tumor in all the xenografted mice (11 out of 11) in a week and showed rapid tumor growth (2784.343 mm^3, n = 11, SD = 922.463, 4 weeks) and dramatic loss of weight (29.49 g on D24 to 27.79 g on D28, n = 11, P = 0.0038, Two-tailed, Paired

t-test), reaching humane end-point in 4 weeks (Fig 1. A-D). The end-point tumor weight was 1.941 g (n = 11, SD = 0.569) (Fig 1. E). Nthy/WT, however, did neither form a tumor nor cause any change to the mice even until two weeks after euthanizing Nthy/V600E-xenografted mice (n = 11). As a result of an autopsy, a little mass of Nthy/WT was found under the skin of the injection site, covered by a fat layer (Fig 1. B). The mean volume was 4.892 mm^3 (n = 10, SD = 2.035, 6 weeks) and that of Nthy/WT was unmeasurable (marked as 0.01 g). The acquired samples of Nthy/V600E and Nthy/WT were formalin-fixed and paraffin-embedded.

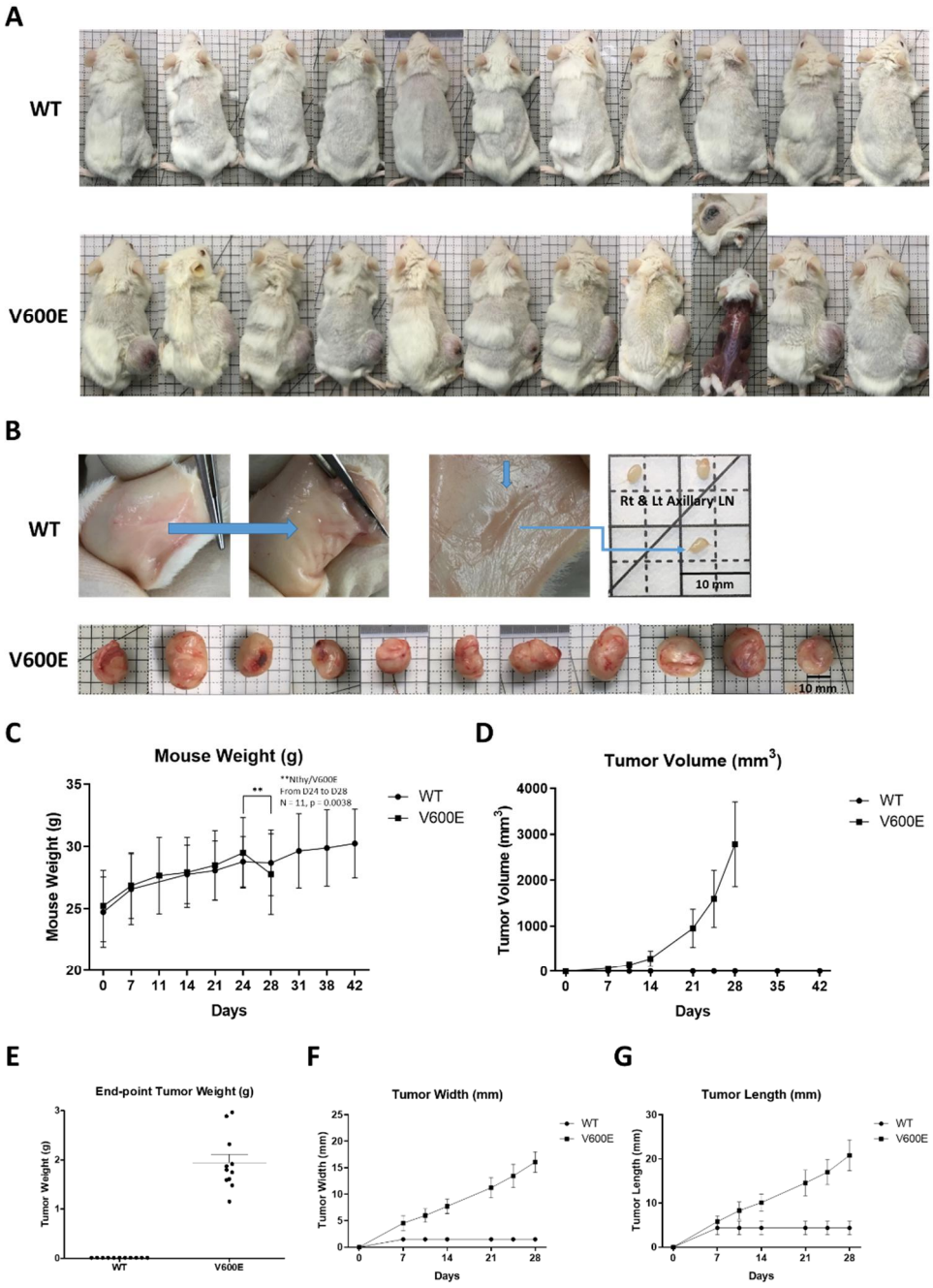

Figure 1. *in vivo* tumorigenesis of SV40-immortalized normal human thyroid epithelial cells initiated by $BRAF^{V600E}$ transduction.

A, B, Nthy/WT or Nthy/V600E-injected mice and the collected tumors at the end point. A, the mice had been monitored for 6 and 4 weeks, respectively. Nthy/WT did not form a tumor without any distinguishable change during the experiments, but Nthy/V600E formed an actively growing tumor on the injection site in all cases. B, a small mass of Nthy/WT under the skin on the injection site was found in an autopsy. It was covered by a fat layer, and in some cases, the mass could not be found. C, significant loss of weight was found

BRAF^{V600E} transduction enables SV40-immortalized normal thyroid cells to metastasize

Because BRAF^{V600E} is known to be associated with poor prognosis of papillary thyroid carcinoma, we have investigated

metastasis in the organs and anatomically relevant lymph nodes with the primary injection site(44). In an anatomy of mice, the primary injection site, the right flank, was between the sciatic lymph node (SaLN) and the subiliac lymph node (SiLN)(45). In the lymphatic drainage system in this region, the lymph flows from SaLN to the proper axillary lymph node (PALN) through the accessory axillary lymph node (AALN) and from SiLN directly to PALN(46, 47). Consequently, if the xenografted cells are metastatic, they are likely to metastasize to SiLN and SaLN first and then to AALN and PALN.

After humane euthanization, we performed an autopsy to find any distinguishable metastatic tumor to the eye. As a result, in all Nthy/V600E-xenografted mice, we found metastatic LNs in both (or either) SaLN and (or) SiLN, with a few exceptions that a primary tumor is big enough to invade the region of the lymph nodes (data are not included). We also found metastasis in the AALN and (or) PALN in 72.7% (8/11) cases, but not in the left axillary LNs (Fig 2. B). However, we could not find any evidence of metastatic LN in Nthy/WT-xenografted mice, and it was confirmed with H&E (Fig 2. A).

In a Nthy/V600E group, metastasis was found not only in

distinguishable metastatic LNs, but also in suspicious and indistinguishable LNs (based on a size) from the right axillary by H&E analysis (Fig 2. B, C). In accordance with the histologic pattern of a primary tumor, metastatic LNs also showed highly pleomorphic nuclei, frequent mitosis, and intranuclear inclusion (Fig 2. A). In H&E analysis of suspicious and indistinguishable LNs from the right and left axillar, the right axillary LN(s) were dotted with or overwhelmed by metastasis of Nthy/V600E depending on the size, but not in the left axillary LN(s) (Fig 2. C).

Moreover, in an additional experiment with 6-8 weeks of incubation (not included in the regular experiment set), we could find a metastasis in the liver (data are not included) and the lung as well, showing that Nthy/V600E is capable of hematogenous distant metastasis to other organs (Fig 2. D).

Based on this data, we concluded that $BRAF^{V600E}$ transduction initiates metastatic ability of a SV40-immortalized normal thyroid cell.

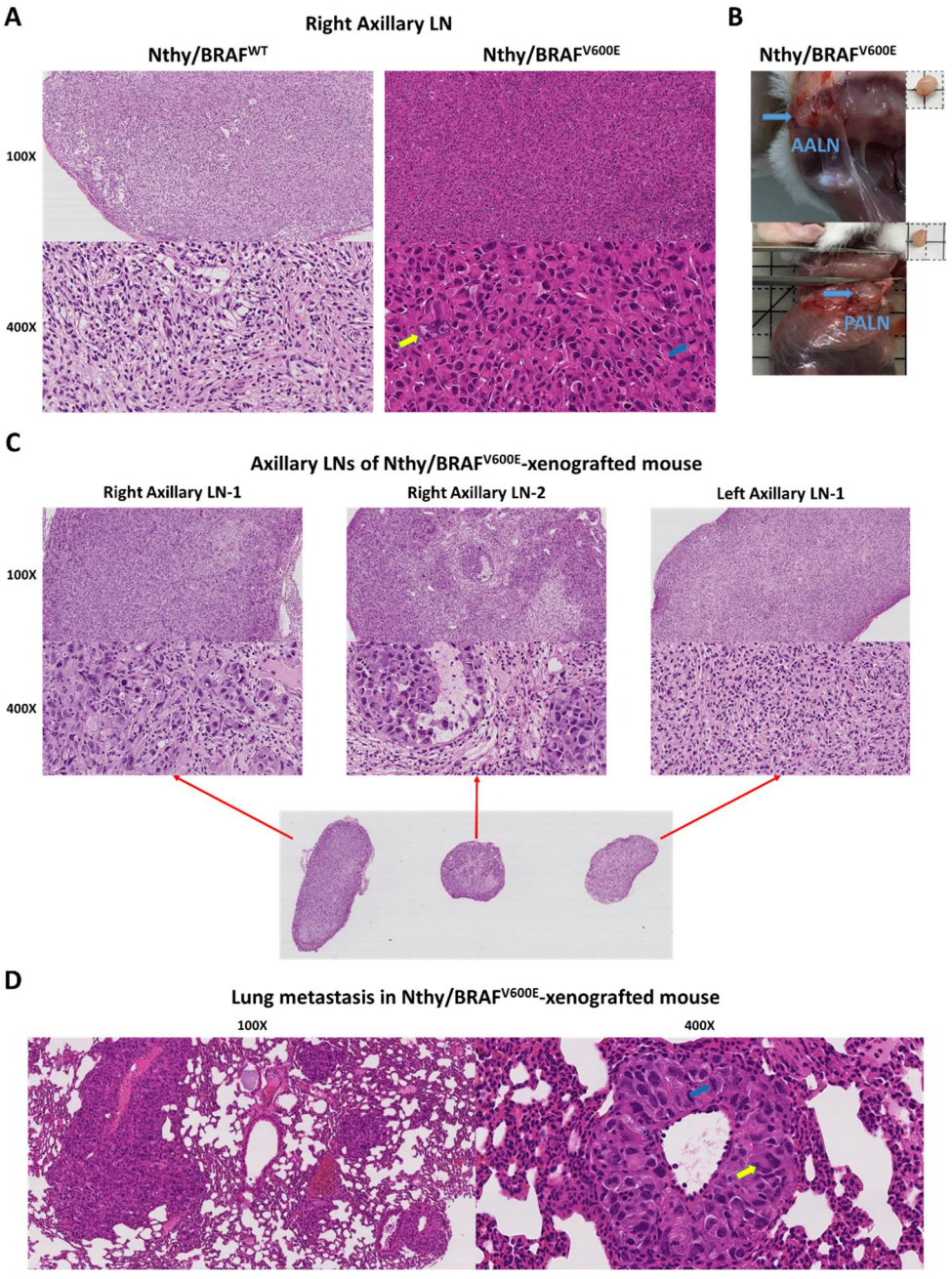
A
Right Axillary LN
Nthy/BRAF^WT
Nthy/BRAF^V600E
100X
400X
B
Nthy/BRAF^V600E
AALN
PALN
C
Axillary LNs of Nthy/BRAF^V600E-xenografted mouse
Right Axillary LN-1
Right Axillary LN-2
Left Axillary LN-1
100X
400X
D
Lung metastasis in Nthy/BRAF^V600E-xenografted mouse
100X
400X

Figure 2. Metastatic characteristics of SV40-immortalized normal thyroid epithelial cells was induced by $BRAF^{V600E}$

A, H&E analysis of right axillary lymph nodes. Lymph node metastasis in observed only in Nthy/V600E while Nthy/WT shows no evidence of metastasis in lymph nodes. Metastatic lymph node of Nthy/V600E showed the same histological features as the primary tumors **B,** metastasis was found in both right AALN (above) and right PALN (below) in Nthy/V600E-xenografted mice. **C,** in Nthy/V600E-xenografted mice, ongoing metastasis was found in right axillary lymph nodes with a small volume. **D,** lung metastasis in Nthy/V600E-xenografted mice was found in an additional set of experiments with 6 weeks of

Treatment of $BRAF^{V600E}$-selective inhibitor PLX-4032 inhibited the growth and metastasis of Nthy/V600E

To confirm that *in vivo* tumorigenesis and metastasis of Nthy/V600E is initiated by $BRAF^{V600E}$, we intraperitoneally treated 10 mg/kg of PLX-4032, which is a $BRAF^{V600E}$-selective inhibitor with FDA approval for $BRAF^{V600E}$-positive late-stage melanoma, from day 14 to day 28 on a daily basis (Fig 3. A).

As a result, compared to the vehicle-treated group (n =3, the mean volume at the end-point was not significantly different from that of the 11 non-treated group), the growth rate of the PLX4032-treated group (n = 6) was significantly decreased ($p < 0.05$) (Fig 3. B, C). However, in a pathologic review by a specialized pathologist, an extra apoptotic region by PLX4032 treatment was not found in H&E analysis (data are not included).

Also, treatment of PLX4032 significantly reduced the volume of metastatic LNs (Fig 3. D). Even though the evidence of metastasis was found regardless of PLX4032 treatment, possibly due to 2 weeks of incubation before treatment, the volume of metastatic LNs was significantly smaller in a PLX4032-treated group (n = 5, 3.43 mm^3) than in a non-treated and vehicle-treated group (n = 11, 23.38 mm^3) ($p = 0.0087$, Mann-Whitney test) (Fig

3. D).

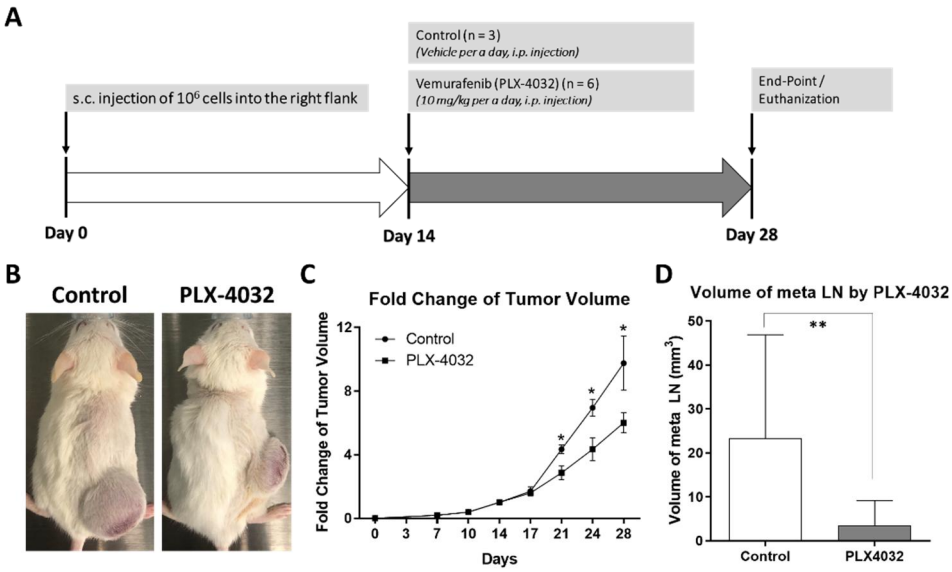

Figure 3. Inhibition of tumor growth and metastasis by $BRAF^{V600E}$-selective inhibitor PLX-4032 (vemurafenib).

A, the overall scheme for PLX-4032 treatment. **B,** Tumor-bearing mice treated with either PLX-4032 or vehicle at the end-point (post-injection 4 weeks, two weeks of drug treatment). **C,** the growth rate of the Nthy/V600E-xenografted tumors was significantly decreased ($*p < 0.05$). **D,** the volume of metastasis in right axillary lymph nodes was significantly smaller in PLX4032-treated group (n = 5) than that in a non-treated and vehicle-treated group (n = 11) ($**p = 0.0087$, Mann-Whitney test).

BRAF^{V600E} transduction induces dedifferentiated thyroid carcinogenesis of SV40-immortalized normal thyroid cells

Because Nthy-ori 3-1 cell line is a normal human thyroid epithelial cells immortalized by transfection of an origin-defective SV40 plasmid, both Nthy/WT and Nthy/V600E are expressing SV40 T-ag, which is known to inactivate p53 and pRb by physically binding.

We first carried out H&E staining of FFPE samples to find out histologic features of Nthy/V600E and Nthy/WT xenografts. In a pathologic review by a pathologist, Nthy/V600E showed highly malignant cellular morphology with marked pleomorphic- and macro-nuclei, frequent mitosis, and intranuclear inclusion (Fig 4. A). On the other hand, Nthy/WT showed monomorphic nuclei and higher fraction of murine stromal cells (Fig 4. A).

In IHC analysis, cytoplasmic expression of BRAF^{V600E} protein in Nthy/V600E is confirmed using anti-BRAFV600E (VE1) antibody (Fig 4. B). Tg and TTF-1 were negative in both Nthy/WT and Nthy/V600E (data are not included), but PAX8 was positive in both, confirming low fraction of Nthy/WT cells in the Nthy/WT xenograft tissue (Fig 4. C). p53 expression was very high in both

Nthy/WT and Nthy/V600E, probably due to structural stabilization by SV40 T-ag (Fig 4. E). To show molecular status on *in vivo* proliferation, expression of Ki67 was analyzed. In accordance with *in vivo* tumor growth rate, Nthy/V600E showed high expression of Ki67 (Fig 4. D). However, even though Nthy/WT was not proliferating *in vivo*, it also showed high Ki67 expression (Fig 4. D). Taken together, a pathologic review of Nthy/V600E tumors by a specialized pathologist was anaplastic thyroid carcinoma.

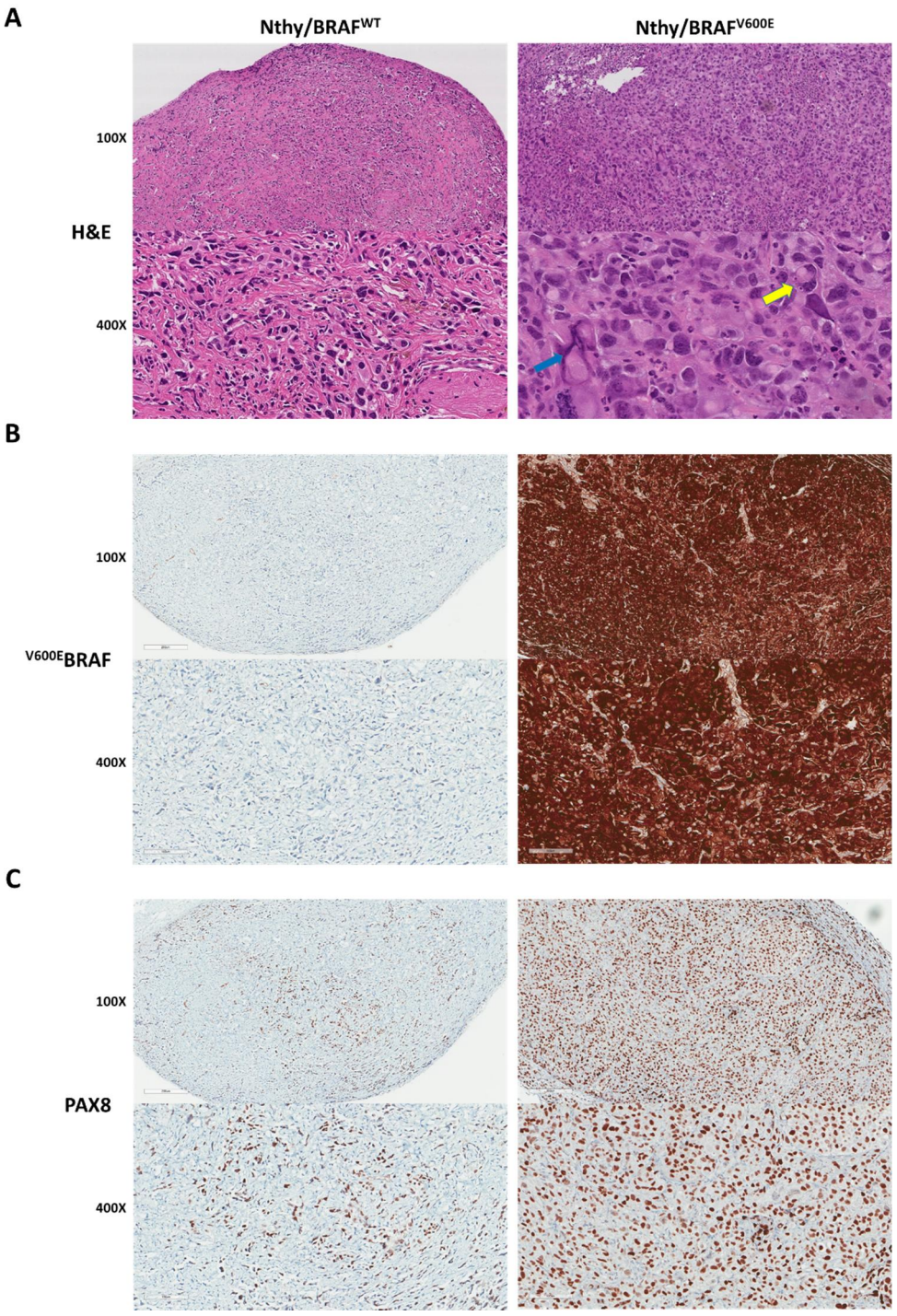
A
Nthy/BRAF^WT
Nthy/BRAF^V600E
100X
H&E
400X
B
100X
V600EBRAF
400X
C
100X
PAX8
400X

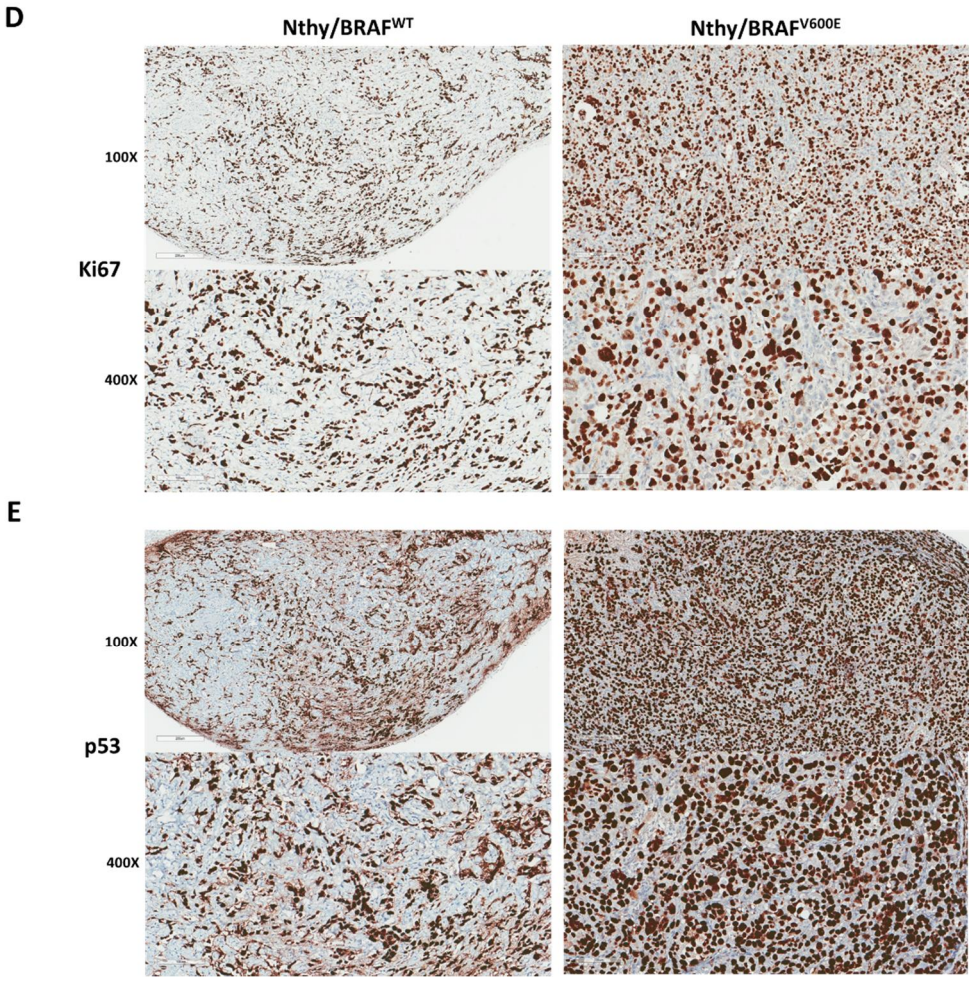

Figure 4. Histological and immunohistochemical phenotypes of SV40-immortalized normal thyroid epithelial cells depending on $BRAF^{V600E}$ status.

A, histological morphology of the xenografted tumors. Nthy/V600E showed highly pleomorphic nuclei, intranuclear inclusion (yellow arrow), and frequent mitosis (blue arrow), but Nthy/WT did not. **B-E,** immunohistochemical features of Nthy/WT and Nthy/V600E. $BRAF^{V600E}$ expression was found only in Nthy/V600E, and PAX8, p53, and Ki67 were highly expressed in both. Tg and TTF-1 expression was negative in both (data are not included). In pathological review by a specialized pathologist, the xenograft tumor of Nthy/V600E was close to anaplastic thyroid carcinoma.

Nthy/V600E shows similar transcriptomic pattern with anaplastic thyroid cancer

To analyze transcriptomic characteristics of Nthy/WT and Nthy/V600E, we used RNA-sequencing and calculated FPKM from mapped reads on UCSC hg19 reference genome. We compared transcriptome of our cell lines with that of the thyroid cell lines available in CCLE and that of human specimens available in GSE33630.

In DEG analysis, we found that there are total 5512 of 2-fold DEGs (up-regulated 1473 and down-regulated 4039 genes, adjusted p-value <0.01) and 3526 4-fold DEGs (up-regulated 627 and down-regulated 2899 genes, adjusted p-value <0.01).

Compared to DEGs between ATC and normal tissues, 295 genes were up-regulated over 2-fold (54 genes, 4-fold), and 571 genes were down-regulated over 2-fold (153 genes, 4-fold) in common (Fig 5. A, B). In gene ontology analysis, the up-regulated genes in common (4-fold) were involved in cell migration, pro-inflammatory signals, immune cell chemotaxis, and extracellular structure organization (Fig 6, Table 1). The down-regulated genes in common(4-fold) were associated with development & morphogenesis of gland, regulation of osteoblast differentiation,

detoxification, inorganic anion transmembrane transport, thyroid hormone generation & metabolic process, hydrogen peroxide metabolic & catabolic process, and apoptotic process (Fig 7, Table 3).

On the other hand, shared DEGs of Nthy/V600E−Nthy/WT with PTC−normal tissues showed 132 (23) up−regulated genes over 2−fold (4−fold) and 135 (18) down−regulated genes over 2−fold (4−fold), which are much less than those with ATC−normal tissues (Fig 5. A, B). The 4−fold up−regulated genes were related to extracellular structure organization, endoderm formation & development, cell adhesion to matrix & substrate, negative regulation of MAPK signaling, immune cell chemotaxis, while the 4−fold down−regulated genes are involved in thyroid hormone generation and metabolic process (Fig 8, 9, Table 2, 4).

In gene expression analysis across thyroid cell lines, we focused on the genes associated with a poor clinical prognosis such as thyroid differentiation, EMT, and cancer prognosis−related genes such as immune checkpoints, EGFR, and VEGF−A.

Overall thyroid differentiation of Nthy/V600E was close to anaplastic thyroid cancer cell lines and even lower than 8305c, which has mutations in *TP53* and *TERT* promoter as well as *BRAF*

(Fig 5. C). However, Nthy/WT showed relatively higher TDS than Nthy/V600E, which is similar with FTC133, but lower than ML1 (Fig 5. C). Although Nthy/WT is not fully differentiated, it expressed the highest level of *SLC5A5* (NIS) and *THRB* (Thyroid hormone receptor beta) among the cell lines, and showed similar or higher expression of all the target genes except *PAX8* than Nthy/V600E (Fig 5. C).

Moreover, Nthy/V600E showed similar expression pattern of EMT-related genes with 8305c (Fig 5. C). It expressed lower level of epithelial signatures such as *CDH1* and *CDH16* and higher level of mesenchymal signatures such as *ZEB1/2*, *CD44*, *TGFbR1*, *SPRY4*, *VIM*, *TWIST1/2*, and *SNAI2* even though several mesenchymal signatures such as *SNAI1*, *CDH2*, and *TGFb* families are lower than Nthy/WT (Fig 5. C).

We selected 9 available genes (excluded genes with zero or near-zero value in all cell lines), which are coding proteins that are getting attention in cancer immunotherapies; immune-stimulatory genes including *TNFSF9* (4-1BBL via 4-1BB) and *CD70* (CD70 via CD27), immune-inhibitory genes including *LGALS3 & 9* (Galectin3 & 9 via TIM-3 and LAG-3), *CD276* (B7-H3 via CD28 family), and *HMGB1* (HMGB1 via TIM-3), and growth factor

pathways such as *EGFR* (EGFR) and *VEGFA* (VEGF-A). Interestingly, Nthy/V600E also showed similar pattern in gene expressions related to cancer immunotherapies with both 8305c and 8505c while showing almost opposite pattern to Nthy/WT (Fig 5. D).

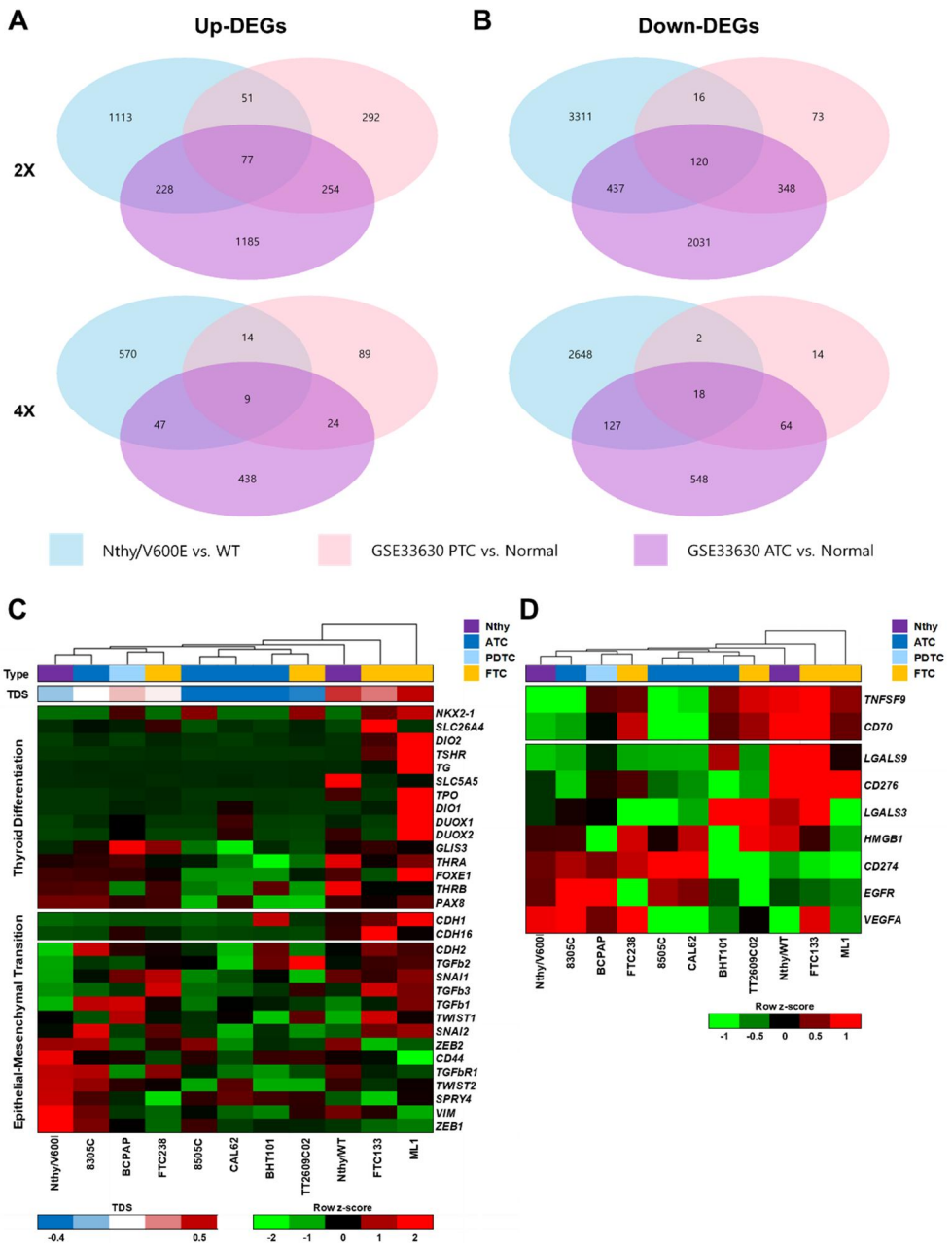

Figure 5. Transcriptomic pattern of Nthy/V600E more corresponds to anaplastic thyroid cancer

A, B, Up- and down-regulated DEGs ($|FC| \geq 2$ or 4, adjusted p-value < 0.01) of Nthy/V600E-Nthy/WT pair with ATC- & PTC-normal tissues pair (GSE33630). Nthy/V600E shared higher proportion of DEGs with ATC than PTC. **C, D,** Hierarchical clustering heat map of gene expressions associated with thyroid differentiation, EMT, and cancer prognosis across human thyroid cell lines. **C,** Nthy/V600E showed as low level of TDS as ATC cell lines, and similar pattern of gene expressions with 8305c cell line. **D,** Like TDS and EMT signatures, it showed similar pattern with 8305c and 8505c.

BRAF^{V600E} transduction activates G1/S phases of SV40-transfected normal thyroid cells

To investigate how BRAF^{V600E} initiates *in vivo* tumorigenesis of SV40-transfected normal human thyroid cells, we cultured the cell lines confluently on a culture dish changing media every day to keep them in fresh media. Because Nthy/WT did not grow *in vivo*, we designed this experiment to induce a contact inhibition *in vitro* considering Nthy/WT shows epithelial morphology and grows in a monolayer while Nthy/V600E is spindle-shaped cells growing in a multilayer on a culture dish(36).

As it has been reported that inhibition p53 and pRb by oncogenic virus such as human papillomavirus (HPV) can result in overexpression of p16^{INK4A} and p21$^{Cip1/WAF1}$ and downregulation of cyclin D1, Nthy/WT showed similar pattern of those gene expression, which was distinctly different from those of other cell lines (Fig 11. A, B, C) (48, 49).

However, BRAF^{V600E} transduction dramatically altered overall expressions of cell cycle-related genes (Fig 10. B). The major components that are important in G1 phase progression such as *CDK4*, *CDK6*, *CCND1* and *CCNE1* except *CDK2* were all increased while *CDKN1A* and *CDKN2A* are dramatically down-

regulated, which are encoding the key G1/S phase arrest protein p21 and p16, respectively (Fig 10. A, B).

On the other hand, G2 phase was relatively inactivated in Nthy/V600E (Fig 10. B). *CDC2* and *CCNB1*, and *CDC25* family were down-regulated with a slight increase in *Wee1*, which inactivates CDK1-Cyclin B1 complex (Fig 10. A, B).

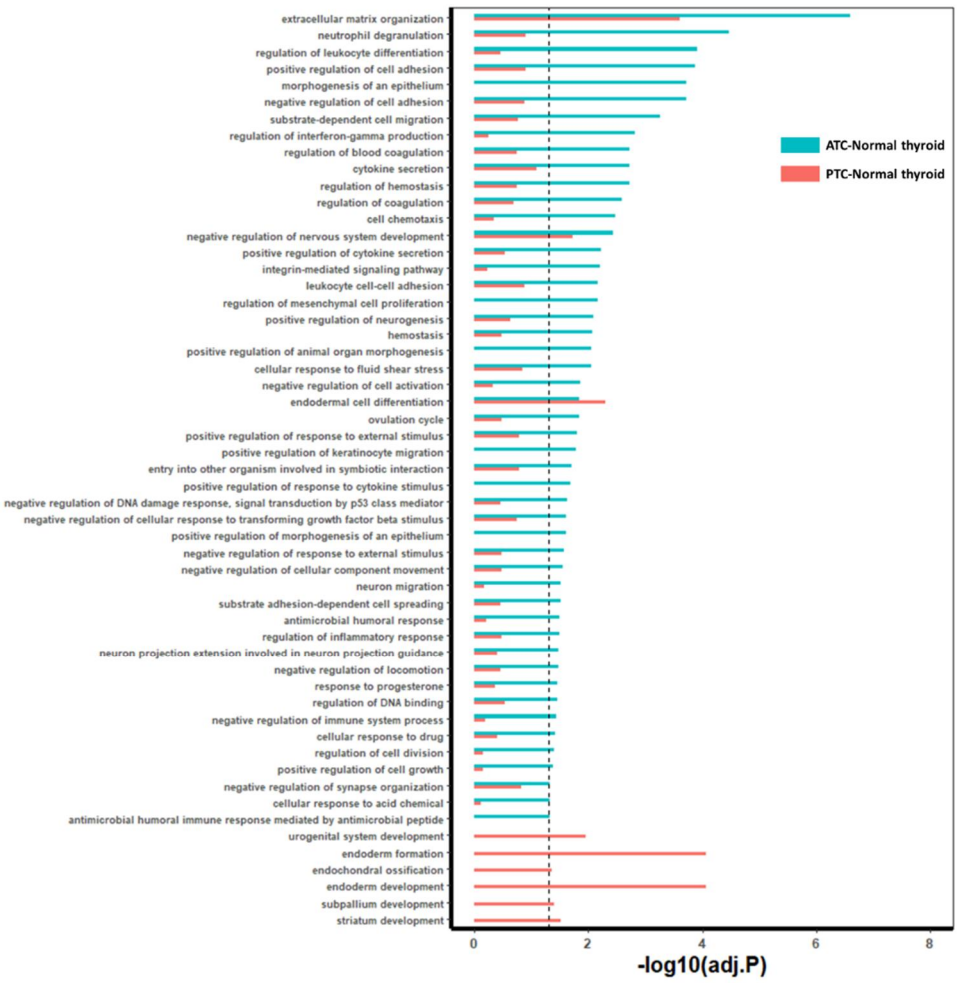

Figure 6. Comparison of Gene Ontology of shared up-regulated DEGs (2-fold) between Nthy/V600E-Nthy/WT and either ATC- or PTC-normal thyroid tissues (GSE33630).

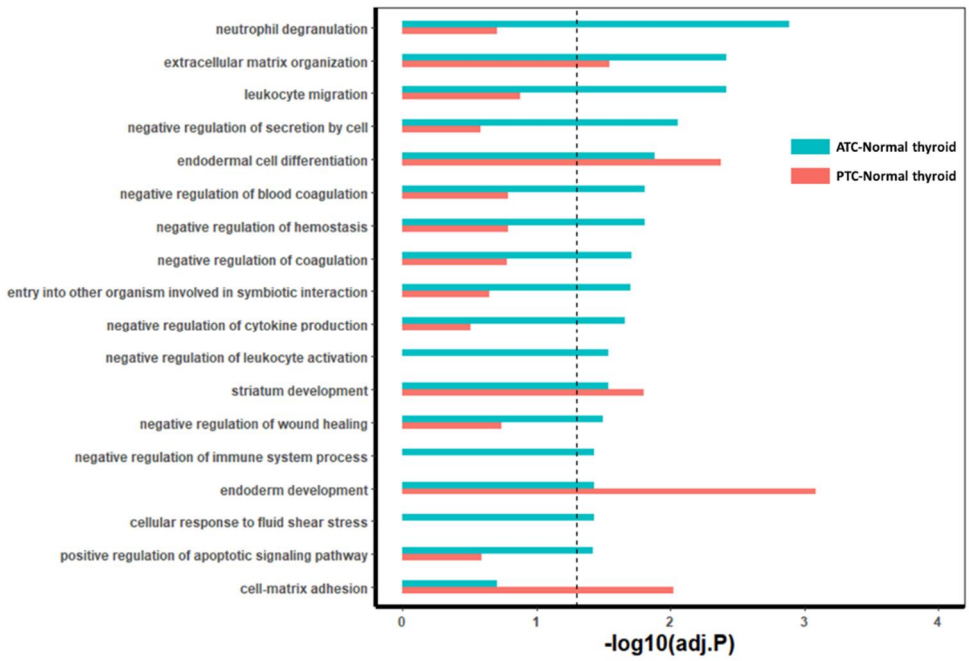

Figure 7. Comparison of Gene Ontology of shared up-regulated DEGs (4-fold) between Nthy/V600E-Nthy/WT and either ATC- or PTC-normal thyroid tissues (GSE33630).

Table 1. List of shared up-regulated DEGs (4-fold) between Nthy/V600E-Nthy/WT and ATC-normal thyroid tissues (GSE33630)

GO Term	Description	Shared DEGs	Count	Adjusted P-value
GO:0030198	extracellular matrix organization	*COL13A1/FN1/HAS2/LAMB3/LOX/MMP1/ADAM19/ADTRP*	8	0.00116
GO:0050900	leukocyte migration	*CCR1/FN1/CXCL1/CXCL2/CXCL3/CXCL8/MMP1/CXCR4/ADTRP*	9	0.00116
GO:0043312	neutrophil degranulation	*ANPEP/CTSC/CR1/CXCL1/LYZ/MME/PLAU/PLAUR/GPR84*	9	0.00116
GO:1903531	negative regulation of secretion by cell	*FN1/IL13RA2/INHBA/PTPN22/TNFRSF21/ADTRP*	6	0.00171
GO:0019730	antimicrobial humoral response	*CXCL1/CXCL2/CXCL3/CXCL8/LYZ*	5	0.00171
GO:0061844	antimicrobial humoral immune response mediated by antimicrobial peptide	*CXCL1/CXCL2/CXCL3/CXCL8*	4	0.00298
GO:0002683	negative regulation of immune system process	*CR1/IL13RA2/INHBA/LY96/PTPN22/TNFRSF21/ADTRP*	7	0.01146
GO:0035987	endodermal cell differentiation	*FN1/INHBA/LAMB3*	3	0.01316
GO:0030195	negative regulation of blood coagulation	*PLAU/PLAUR/ADTRP*	3	0.01582
GO:1900047	negative regulation of hemostasis	*PLAU/PLAUR/ADTRP*	3	0.01582
GO:0050819	negative regulation of coagulation	*PLAU/PLAUR/ADTRP*	3	0.01636
GO:0051828	entry into other organism involved in symbiotic interaction	*ANPEP/CR1/CXCL8/CXCR4*	4	0.01636
GO:0022407	regulation of cell-cell adhesion	*HAS2/ADAM19/PTPN22/TNFRSF21/FXYD5/ADTRP*	6	0.02071
GO:0001818	negative regulation of cytokine production	*FN1/INHBA/PTPN22/TNFRSF21/NAV3*	5	0.02071
GO:0061045	negative regulation of wound healing	*PLAU/PLAUR/ADTRP*	3	0.02794
GO:0002695	negative regulation of leukocyte activation	*IL13RA2/INHBA/PTPN22/TNFRSF21*	4	0.02901
GO:0007492	endoderm development	*FN1/INHBA/LAMB3*	3	0.02901
GO:0021756	striatum development	*ALDH1A3/INHBA*	2	0.02953
GO:2001235	positive regulation of apoptotic signaling pathway	*CTSC/INHBA/PLAUR/G0S2*	4	0.02953
GO:0071498	cellular response to fluid shear stress	*HAS2/TFPI2*	2	0.03354
GO:0051224	negative regulation of protein transport	*FN1/PTPN22/TNFRSF21/ADTRP*	4	0.03400
GO:0051701	interaction with host	*ANPEP/CR1/CXCL8/CXCR4*	4	0.04508

Table 2. List of shared up-regulated DEGs (4-fold) between Nthy/V600E-Nthy/WT and PTC-normal thyroid tissues (GSE33630).

GO Term	Description	Shared DEGs	Count	Adjusted P-value
GO:0007160	cell-matrix adhesion	*COL13A1/FN1/PLAU/ADAMTS9*	4	0.03256
GO:0021756	striatum development	*ALDH1A3/LRRK2*	2	0.04467

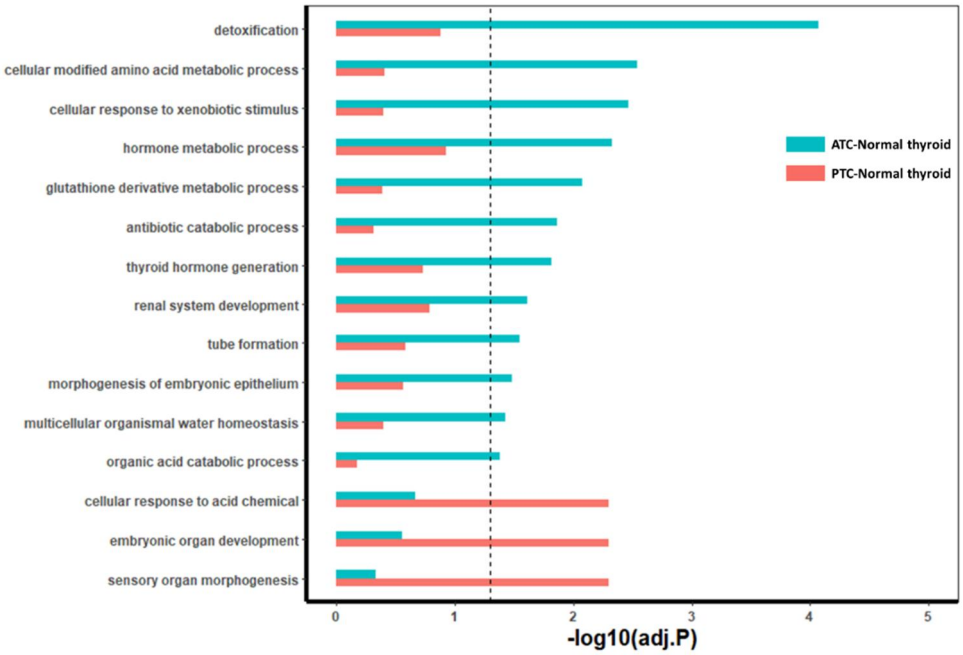

Figure 8. Comparison of Gene Ontology of shared down-regulated DEGs (2-fold) between Nthy/V600E-Nthy/WT and either ATC- or PTC-normal thyroid tissues (GSE33630).

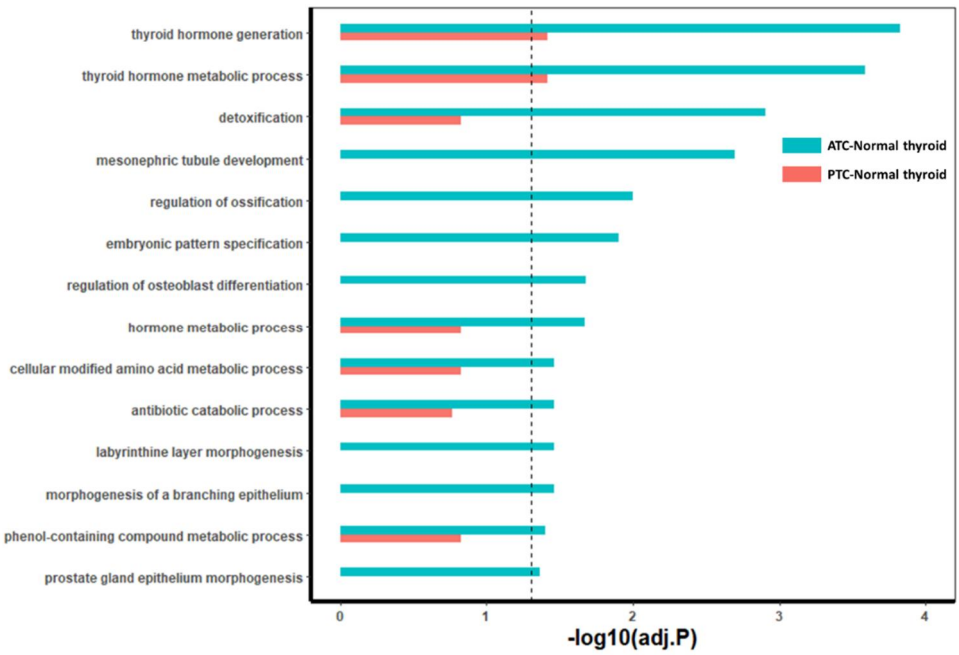

Figure 9. Comparison of Gene Ontology of shared down-regulated DEGs (4-fold) between Nthy/V600E-Nthy/WT and either ATC- or PTC-normal thyroid tissues (GSE33630).

Table 3. List of shared down-regulated DEGs (4-fold) between Nthy/V600E-Nthy/WT and ATC-normal thyroid tissues (GSE33630).

GO Term	Description	Shared DEGs	Count	Adjusted P-value
GO:0006590	thyroid hormone generation	*DIO2/TPO/DUOX2/DUOX1/DUOXA1*	5	0.00014
GO:0098754	detoxification	*BMP7/GPX3/MT1F/PON3/SOD3/TPO/DUOX2/DUOX1*	8	0.00167
GO:0072164	mesonephric tubule development	*BMP7/FGFR2/EPCAM/SMAD6/PBX1/PGF/NPNT*	7	0.00167
GO:0045667	regulation of osteoblast differentiation	*BMP7/FGFR2/ID4/LRP5/LTF/SMAD6/NPNT*	7	0.00501
GO:0030278	regulation of ossification	*BMP7/FGFR2/ID4/LRP5/LTF/SMAD6/PBX1/NPNT*	8	0.00961
GO:0009880	embryonic pattern specification	*BMP7/ERBB4/FGFR2/SMAD6/COBL*	5	0.00961
GO:0042445	hormone metabolic process	*CPE/CRABP1/DIO2/PON3/TPO/DUOX2/DUOX1/DUOXA1*	8	0.01510
GO:0061138	morphogenesis of a branching epithelium	*BMP7/FGFR2/LRP5/PBX1/PGF/SPINT2/NPNT*	7	0.02586
GO:0060713	labyrinthine layer morphogenesis	*BMP7/FGFR2/SPINT2*	3	0.02931
GO:0006575	cellular modified amino acid metabolic process	*ASS1/DIO2/FOLR1/TPO/DUOX2/DUOX1/DUOXA1*	7	0.03273
GO:0018958	phenol-containing compound metabolic process	*DIO2/TPO/DUOX2/DUOX1/DUOXA1*	5	0.03687
GO:0017001	antibiotic catabolic process	*GPX3/TPO/DUOX2/DUOX1*	4	0.03688
GO:0060740	prostate gland epithelium morphogenesis	*BMP7/FGFR2/ID4*	3	0.03885
GO:0001649	osteoblast differentiation	*BMP7/FGFR2/ID4/LRP5/LTF/SMAD6/NPNT*	7	0.03885

Table 4. List of shared down-regulated DEGs (4-fold) between Nthy/V600E-Nthy/WT and PTC-normal thyroid tissues (GSE33630).

GO Term	Description	Shared DEGs	Count	Adjusted P-value
GO:0006590	thyroid hormone generation	*DIO2/TPO*	2	0.04017
GO:0042403	thyroid hormone metabolic process	*DIO2/TPO*	2	0.04017

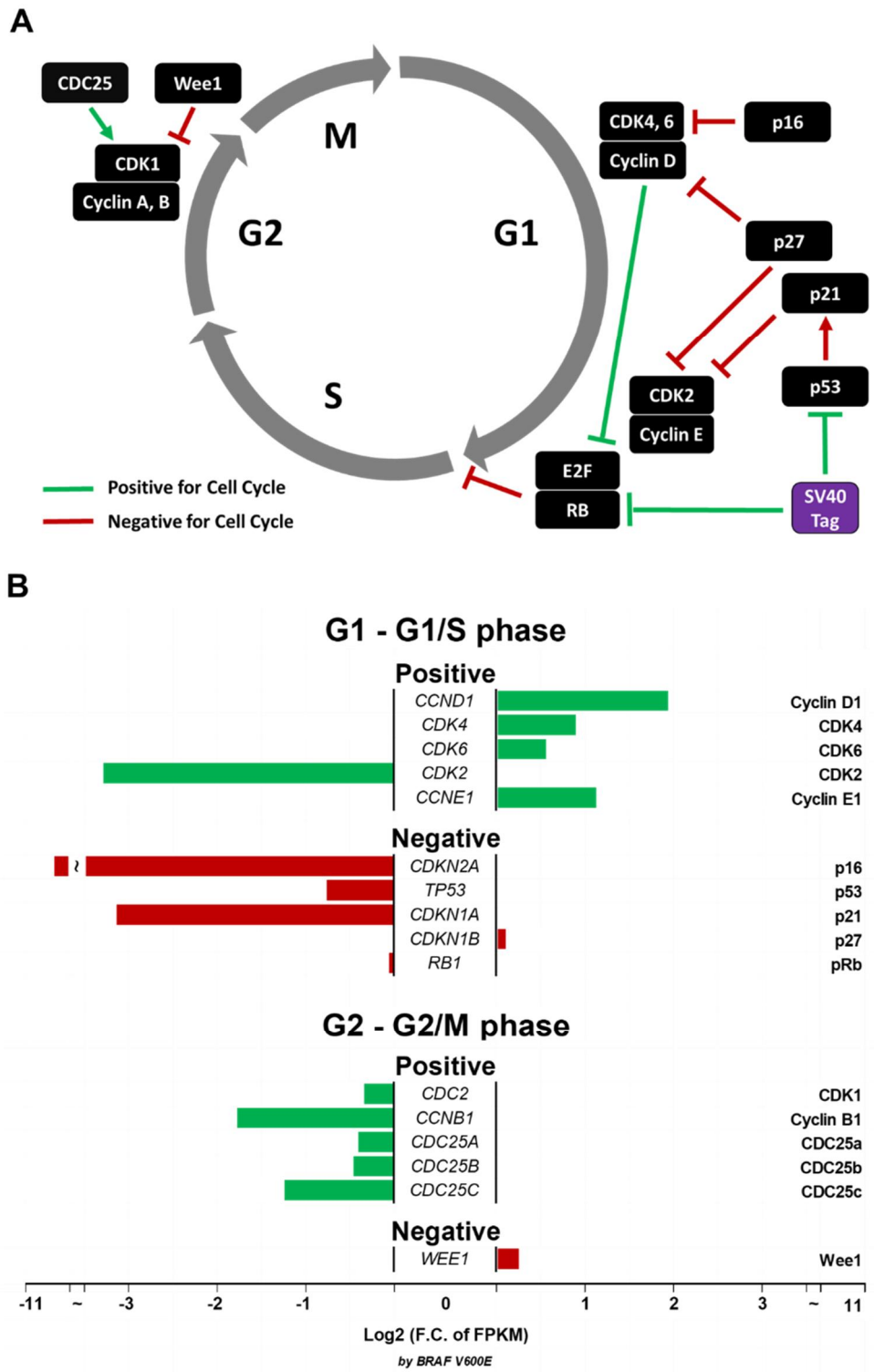
A
CDC25
Wee1
CDK1
Cyclin A, B
M
G2
G1
S
CDK4, 6
Cyclin D
p16
p27
p21
p53
CDK2
Cyclin E
E2F
RB
SV40
Tag
Positive for Cell Cycle
Negative for Cell Cycle
B
G1 - G1/S phase
Positive
CCND1
CDK4
CDK6
CDK2
CCNE1
Cyclin D1
CDK4
CDK6
CDK2
Cyclin E1
Negative
CDKN2A
TP53
CDKN1A
CDKN1B
RB1
p16
p53
p21
p27
pRb
G2 - G2/M phase
Positive
CDC2
CCNB1
CDC25A
CDC25B
CDC25C
CDK1
Cyclin B1
CDC25a
CDC25b
CDC25c
Negative
WEE1
Wee1
-11
~
-3
-2
-1
0
1
2
3
~
11
Log2 (F.C. of FPKM)
by BRAF V600E

Figure 10. Regulation of cell cycle-associated gene expression by $BRAF^{V600E}$ in SV40-transfected normal human thyroid cells

A, A schematic diagram of cell cycle regulation in SV40-transfected cells. Green lines stand for promotion of cell cycle, and red lines represent inhibitory signaling of cell cycle(1-7). **B,** Relative expression of cell cycle-associated genes in Nthy/V600E over Nthy/WT in a confluently cultured condition. In a fully cultured condition, G1 and G1/S phase-promoting signals were relatively activated in Nthy/V600E while G2 and G2/M phase-signals were relatively inactivated.

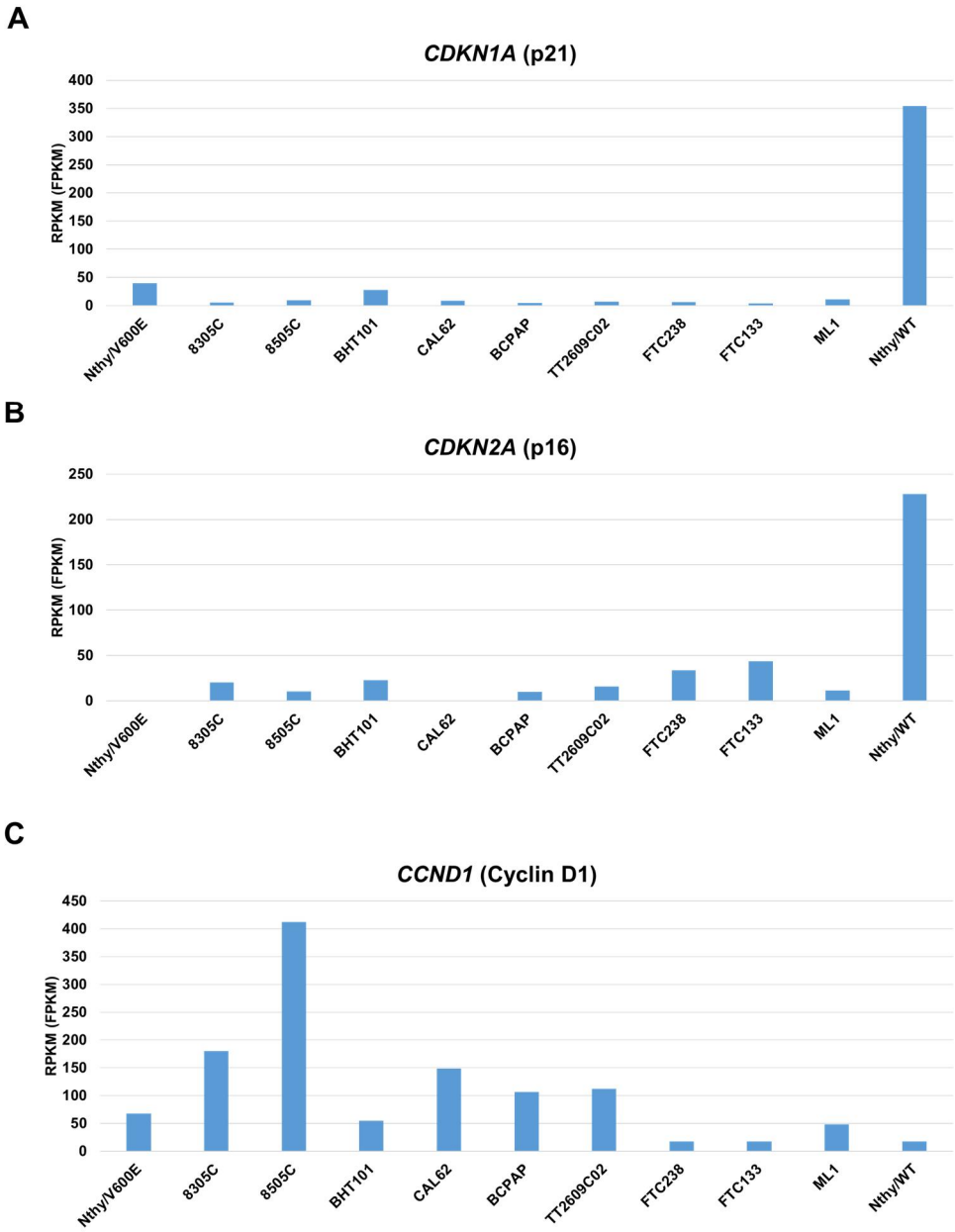

Figure 11. Relative expression (RPKM or FPKM) of CDKN1A, CDKN2A, and CCND1 across the used human thyroid cell lines

Discussion

We have successfully established a new xenograft model for $BRAF^{V600E}$-positive human dedifferentiated thyroid carcinoma by transducing SV40-transfected normal human thyroid cells with $BRAF^{V600E}$. As it was previously reported that Nthy-ori 3-1 is not tumorigenic in immunodeficient nude mice in the original article, SV40 was not solely able to induce *in vivo* tumorigenesis of a normal human thyroid cell even in NSG mice, which does have little immunity (41). Unlike the murine PTC model induced by thyroid-specific expression of $BRAF^{V600E}$, Nthy/V600E formed dedifferentiated thyroid cancer showing very poor differentiation status and aggressive behaviors *in vivo* (50).

Nthy/V600E metastasized to both relevant LNs and distant organs. In an anatomy of mice, the primary injection site, the right flank, was between the SaLN and the SiLN (45). In the lymphatic drainage system in this region, the lymph flows from the SaLN to the PALN through the AALN and from the SiLN directly to the PALN (46, 47). This would be the reason that metastatic LNs are found in the right axillary LNs, not in the left ones.

Even though Nthy-ori 3-1 as well as Nthy/WT was not tumorigenic *in vivo* and these cell lines are a 'normal' cell line,

our data and other previous reports using Nthy-ori 3-1 showed that this cell line expresses no or low level of thyroid-specific markers, meaning that it might not be in a well-differentiated status (51). Among possible reasons for this ironic phenotype, one might be because this cell line has long been cultured in vitro with numerous passages, but it might better explain the low differentiation status of Nthy-ori 3-1 that p53 and pRb inactivation by SV40 transfection played an important role in its differentiation status considering mutations in p53 and pRb are more frequently found in advanced thyroid carcinomas (27). Considering that $BRAF^{V600E}$ expression was solely able to initiate an adult-onset papillary thyroid carcinoma in a genetically engineered mouse model, Nthy/V600E might also form papillary thyroid cancer if SV40 is completely inhibited (29, 50).

Presence of SV40 in thyroid cancer tissues has been reported by Vivaldi et al. In the study, SV40 T-ag mRNA was detected in 69% (9/13) of PTC and in 73% (8/11) of ATC, but expression of T-ag protein was found in only 33% (3/9) of mRNA-detected PTC and 100% (8/8) of mRNA-detected ATC (39). Further researches to confirm clinical importance of SV40 T-ag would be required to utilize detection of SV40 T-ag in a combination with $BRAF^{V600E}$ in fine needle aspiration specimens to

predict aggressive subtypes of thyroid cancers in a pre-surgical diagnosis.

We analyzed cell cycle-related genes, mainly the ones regulated by the level of expression to find a clue for molecular pathogenesis of $BRAF^{V600E}$ in our model. In this analysis, we compared only Nthy/WT and Nthy/V600E because genes involved in a cell cycle might be critically affected by a culture condition, especially when they are cultured with a full confluency like our case.

Nthy/WT showed similar pattern with human papillomavirus (HPV)-infected tonsillar squamous cell carcinoma with a favorable clinical outcome (49). HPV is one of the well-known oncogenic virus causing cancer or precancerous lesions in multiple regions in our body by inhibiting p53 and pRb via HPV E6 and E7 oncoproteins(52). According to the report by Hafkamp et al. in 2009, tonsillar squamous cell carcinoma showed significantly higher expression of p21 and and p16 in HPV-infected cases and p21-overexpression is strongly associated with a good prognosis (49).

However, $BRAF^{V600E}$ transduction dramatically decreased *CDKN1A* and *CDKN2A* expression until similar level with other cancer cell lines (Supp. Fig 5. A, B). It is very interesting

considering the two things: First, p21 is rarely detected in ATC, but not in well-differentiated thyroid cancers (53). Second, HPV induces both benign and malignant tumors, and HPV-positive tumors have better prognosis than that of HPV-negative tumors (52). Considering that Salerno et al. and Sala et al. showed $BRAF^{V600E}$ inhibition up-regulates *CDKN1A* in $BRAF^{V600E}$-mutated thyroid cancer cell lines, *CDKN1A* might be a key molecule in $BRAF^{V600E}$-induced carcinogenesis (54, 55). However, because we only screened at the mRNA level and has not proved it experimentally yet, more studies to reveal the underlying mechanism would be needed for therapeutic application.

The critical limitation of our model in this aspect is that the backbone cell line Nthy-ori 3-1 expresses origin-defective SV40 proteins such as SV40 T-ag, leaving a question that carcinogenesis of normal human thyrocytes by $BRAF^{V600E}$ transduction might be dependent on the presence of SV40-originated oncoproteins. Further investigations such as inhibition of SV40 proteins would be required to prove that $BRAF^{V600E}$ is solely able to induce carcinogenesis of normal thyroid epithelial cells in human as Charles et al. showed in a murine thyroid epithelial cells.

In conclusion, our data show that $BRAF^{V600E}$ plays a crucial

role in the induction of carcinogenesis of a normal human thyroid cell line activating ATC-like cellular signaling pathways. Although p53 and pRb inhibition by SV40 T-ag might also contribute to the carcinogenesis of a normal human thyroid epithelial cell in this model, it is obvious that $BRAF^{V600E}$ is essential for *in vivo* tumorigenesis even in the transformed cells by SV40 by activating G1 phase and promoting progression to S phase. Therefore, we expect that this mouse xenograft model of human dedifferentiated thyroid cancer mediated by $BRAF^{V600E}$ and SV40 would contribute to further researches on the etiopathogenesis of thyroid carcinomas and targeted therapies for BRAF-mutated thyroid cancer patients.

References

1. Cayrol C, Knibiehler M, Ducommun B. p21 binding to PCNA causes G1 and G2 cell cycle arrest in p53-deficient cells. Oncogene. 1998;16(3):311-20.
2. Pipas JM. SV40: Cell transformation and tumorigenesis. Virology. 2009;384(2):294-303.
3. Chen J. The Cell-Cycle Arrest and Apoptotic Functions of p53 in Tumor Initiation and Progression. Cold Spring Harb Perspect Med. 2016;6(3):a026104.
4. Goodrich DW, Wang NP, Qian YW, Lee EY, Lee WH. The retinoblastoma gene product regulates progression through the G1 phase of the cell cycle. Cell. 1991;67(2):293-302.
5. Meyerson M, Harlow E. Identification of G1 kinase activity for cdk6, a novel cyclin D partner. Mol Cell Biol. 1994;14(3):2077-86.
6. Den Haese GJ, Walworth N, Carr AM, Gould KL. The Wee1 protein kinase regulates T14 phosphorylation of fission yeast Cdc2. Mol Biol Cell. 1995;6(4):371-85.
7. Schafer KA. The cell cycle: a review. Vet Pathol. 1998;35(6):461-78.
8. Lee JH, Shin SW. Overdiagnosis and screening for thyroid cancer in Korea. Lancet. 2014;384(9957):1848.
9. Cancer Genome Atlas Research N. Integrated genomic characterization of papillary thyroid carcinoma. Cell. 2014;159(3):676-90.
10. Xu B, Ghossein R. Evolution of the histologic classification of thyroid neoplasms and its impact on clinical management. Eur J Surg Oncol. 2018;44(3):338-47.
11. Correa P, Chen VW. Endocrine gland cancer. Cancer. 1995;75(1 Suppl):338-52.
12. Liu Z, Zeng W, Huang L, Wang Z, Wang M, Zhou L, et al. Prognosis of FTC compared to PTC and FVPTC: findings based on SEER database using propensity score matching analysis. Am J Cancer Res. 2018;8(8):1440-8.
13. Edge SB, Compton CC. The American Joint Committee on Cancer: the

7th edition of the AJCC cancer staging manual and the future of TNM. Ann Surg Oncol. 2010;17(6):1471-4.

14. Wada N, Duh QY, Miura D, Brunaud L, Wong MG, Clark OH. Chromosomal aberrations by comparative genomic hybridization in hurthle cell thyroid carcinomas are associated with tumor recurrence. J Clin Endocrinol Metab. 2002;87(10):4595-601.

15. Stamatakos M, Paraskeva P, Stefanaki C, Katsaronis P, Lazaris A, Safioleas K, et al. Medullary thyroid carcinoma: The third most common thyroid cancer reviewed. Oncol Lett. 2011;2(1):49-53.

16. Barbet J, Campion L, Kraeber-Bodere F, Chatal JF, Group GTES. Prognostic impact of serum calcitonin and carcinoembryonic antigen doubling-times in patients with medullary thyroid carcinoma. J Clin Endocrinol Metab. 2005;90(11):6077-84.

17. Pita JM, Banito A, Cavaco BM, Leite V. Gene expression profiling associated with the progression to poorly differentiated thyroid carcinomas. Br J Cancer. 2009;101(10):1782-91.

18. Mogos IC, Niculescu DA, Ioachim D, Iorgulescu R, Poiana C. Overall Survival of Patients with Aggressive Thyroid Cancer on Fine-Needle Aspiration Biopsy Examination. A Tertiary Romanian Center Experience. Maedica (Buchar). 2015;10(3):221-5.

19. Haddad RI, Lydiatt WM, Ball DW, Busaidy NL, Byrd D, Callender G, et al. Anaplastic Thyroid Carcinoma, Version 2.2015. J Natl Compr Canc Netw. 2015;13(9):1140-50.

20. Bishop JA, Sharma R, Westra WH. PAX8 immunostaining of anaplastic thyroid carcinoma: a reliable means of discerning thyroid origin for undifferentiated tumors of the head and neck. Hum Pathol. 2011;42(12):1873-7.

21. Subbiah V, Kreitman RJ, Wainberg ZA, Cho JY, Schellens JHM, Soria JC, et al. Dabrafenib and Trametinib Treatment in Patients With Locally Advanced or Metastatic BRAF V600-Mutant Anaplastic Thyroid Cancer. J Clin Oncol. 2018;36(1):7-13.

22. Lee SE, Hwang TS, Choi YL, Kim WY, Han HS, Lim SD, et al. Molecular Profiling of Papillary Thyroid Carcinoma in Korea with a High Prevalence of BRAF(V600E) Mutation. Thyroid. 2017;27(6):802-10.

23. Xing M, Alzahrani AS, Carson KA, Shong YK, Kim TY, Viola D, et al. Association between BRAF V600E mutation and recurrence of papillary thyroid cancer. J Clin Oncol. 2015;33(1):42-50.

24. Xing M, Alzahrani AS, Carson KA, Viola D, Elisei R, Bendlova B, et al. Association between BRAF V600E mutation and mortality in patients with papillary thyroid cancer. JAMA. 2013;309(14):1493-501.
25. Yoo SK, Lee S, Kim SJ, Jee HG, Kim BA, Cho H, et al. Comprehensive Analysis of the Transcriptional and Mutational Landscape of Follicular and Papillary Thyroid Cancers. PLoS Genet. 2016;12(8):e1006239.
26. Kroll TG, Sarraf P, Pecciarini L, Chen CJ, Mueller E, Spiegelman BM, et al. PAX8-PPARgamma1 fusion oncogene in human thyroid carcinoma [corrected]. Science. 2000;289(5483):1357-60.
27. Pozdeyev N, Gay LM, Sokol ES, Hartmaier R, Deaver KE, Davis S, et al. Genetic Analysis of 779 Advanced Differentiated and Anaplastic Thyroid Cancers. Clin Cancer Res. 2018;24(13):3059-68.
28. Liu R, Zhang T, Zhu G, Xing M. Regulation of mutant TERT by BRAF V600E/MAP kinase pathway through FOS/GABP in human cancer. Nat Commun. 2018;9(1):579.
29. McFadden DG, Vernon A, Santiago PM, Martinez-McFaline R, Bhutkar A, Crowley DM, et al. p53 constrains progression to anaplastic thyroid carcinoma in a Braf-mutant mouse model of papillary thyroid cancer. Proc Natl Acad Sci U S A. 2014;111(16):E1600-9.
30. Xing M, Liu R, Liu X, Murugan AK, Zhu G, Zeiger MA, et al. BRAF V600E and TERT promoter mutations cooperatively identify the most aggressive papillary thyroid cancer with highest recurrence. J Clin Oncol. 2014;32(25):2718-26.
31. Song YS, Lim JA, Choi H, Won JK, Moon JH, Cho SW, et al. Prognostic effects of TERT promoter mutations are enhanced by coexistence with BRAF or RAS mutations and strengthen the risk prediction by the ATA or TNM staging system in differentiated thyroid cancer patients. Cancer. 2016;122(9):1370-9.
32. Liu C, Liu Z, Chen T, Zeng W, Guo Y, Huang T. TERT promoter Mutation and Its Association with Clinicopathological Features and Prognosis of Papillary Thyroid Cancer: A Meta-analysis. Sci Rep. 2016;6:36990.
33. Saiselet M, Floor S, Tarabichi M, Dom G, Hebrant A, van Staveren WC, et al. Thyroid cancer cell lines: an overview. Front Endocrinol (Lausanne). 2012;3:133.
34. Henderson YC, Ahn SH, Ryu J, Chen Y, Williams MD, El-Naggar AK, et al. Development and characterization of six new human papillary thyroid carcinoma cell lines. J Clin Endocrinol Metab. 2015;100(2):E243-52.

35. Vanden Borre P, McFadden DG, Gunda V, Sadow PM, Varmeh S, Bernasconi M, et al. The next generation of orthotopic thyroid cancer models: immunocompetent orthotopic mouse models of BRAF V600E-positive papillary and anaplastic thyroid carcinoma. Thyroid. 2014;24(4):705-14.
36. Kim BA, Jee HG, Yi JW, Kim SJ, Chai YJ, Choi JY, et al. Expression Profiling of a Human Thyroid Cell Line Stably Expressing the BRAFV600E Mutation. Cancer Genomics Proteomics. 2017;14(1):53-67.
37. Poulin DL, DeCaprio JA. Is there a role for SV40 in human cancer? J Clin Oncol. 2006;24(26):4356-65.
38. Pacini F, Vivaldi A, Santoro M, Fedele M, Fusco A, Romei C, et al. Simian virus 40-like DNA sequences in human papillary thyroid carcinomas. Oncogene. 1998;16(5):665-9.
39. Vivaldi A, Pacini F, Martini F, Iaccheri L, Pezzetti F, Elisei R, et al. Simian virus 40-like sequences from early and late regions in human thyroid tumors of different histotypes. J Clin Endocrinol Metab. 2003;88(2):892-9.
40. Ozdarendeli A, Camci C, Aygen E, Kirkil C, Toroman ZA, Dogru O, et al. SV40 in human thyroid nodules. J Clin Virol. 2004;30(4):337-40.
41. Lemoine NR, Mayall ES, Jones T, Sheer D, McDermid S, Kendall-Taylor P, et al. Characterisation of human thyroid epithelial cells immortalised in vitro by simian virus 40 DNA transfection. British Journal of Cancer. 1989;60(6):897-903.
42. Kim D, Langmead B, Salzberg SL. HISAT: a fast spliced aligner with low memory requirements. Nat Methods. 2015;12(4):357-60.
43. Pertea M, Pertea GM, Antonescu CM, Chang TC, Mendell JT, Salzberg SL. StringTie enables improved reconstruction of a transcriptome from RNA-seq reads. Nat Biotechnol. 2015;33(3):290-5.
44. Xing M. BRAF mutation in papillary thyroid cancer: pathogenic role, molecular bases, and clinical implications. Endocr Rev. 2007;28(7):742-62.
45. Van den Broeck W, Derore A, Simoens P. Anatomy and nomenclature of murine lymph nodes: Descriptive study and nomenclatory standardization in BALB/cAnNCrl mice. J Immunol Methods. 2006;312(1-2):12-9.
46. Kodama T, Hatakeyama Y, Kato S, Mori S. Visualization of fluid drainage pathways in lymphatic vessels and lymph nodes using a mouse model to test a lymphatic drug delivery system. Biomed Opt Express. 2015;6(1):124-34.
47. Nakajima Y, Asano K, Mukai K, Urai T, Okuwa M, Sugama J, et al. Near-Infrared Fluorescence Imaging Directly Visualizes Lymphatic Drainage Pathways and Connections between Superficial and Deep Lymphatic Systems in the

Mouse Hindlimb. Sci Rep. 2018;8(1):7078.
48. Rabban JT SR, Zaloudek CZ. Immunohistology of the Female Genital Tract. Diagnostic Immunohistochemistry [Internet]. Elsevier. 2010:690–762.
49. Hafkamp HC, Mooren JJ, Claessen SM, Klingenberg B, Voogd AC, Bot FJ, et al. P21 Cip1/WAF1 expression is strongly associated with HPV-positive tonsillar carcinoma and a favorable prognosis. Mod Pathol. 2009;22(5):686-98.
50. Charles RP, Iezza G, Amendola E, Dankort D, McMahon M. Mutationally activated BRAF(V600E) elicits papillary thyroid cancer in the adult mouse. Cancer Res. 2011;71(11):3863-71.
51. Espadinha C, Cavaco BM, Leite V. PAX8PPARgamma stimulates cell viability and modulates expression of thyroid-specific genes in a human thyroid cell line. Thyroid. 2007;17(6):497-509.
52. Fakhry C, Gillison ML. Clinical implications of human papillomavirus in head and neck cancers. J Clin Oncol. 2006;24(17):2606-11.
53. Smallridge RC, Copland JA. Anaplastic thyroid carcinoma: pathogenesis and emerging therapies. Clin Oncol (R Coll Radiol). 2010;22(6):486-97.
54. Salerno P, De Falco V, Tamburrino A, Nappi TC, Vecchio G, Schweppe RE, et al. Cytostatic activity of adenosine triphosphate-competitive kinase inhibitors in BRAF mutant thyroid carcinoma cells. J Clin Endocrinol Metab. 2010;95(1):450-5.
55. Sala E, Mologni L, Truffa S, Gaetano C, Bollag GE, Gambacorti-Passerini C. BRAF silencing by short hairpin RNA or chemical blockade by PLX4032 leads to different responses in melanoma and thyroid carcinoma cells. Mol Cancer Res. 2008;6(5):751-9.

국문 초록

배경: $BRAF^{V600E}$는 갑상선암에서 가장 높은 빈도로 발견되는 돌연변이다. 최초로 발견된 이후 $BRAF^{V600E}$의 임상학적 중요성에 대해서 활발한 연구가 진행되어 왔지만, 갑상선암의 원인병리론에 미치는 $BRAF^{V600E}$의 역할을 연구하기 위한 적합한 연구모델은 아직 구축된 바 없다. $BRAF^{V600E}$이 인간 갑상선암 발생에 미치는 역할을 연구하고 $BRAF^{V600E}$를 발현하는 인간 갑상선암을 연구하기 위한 새로운 동물실험모델을 구축하기 위해, 폴리오마 바이러스의 일종인 SV40를 이용해 불멸화시킨 인간 정상 갑상선 세포주 Nthy-ori 3-1을 렌티바이러스로 $BRAF^{WT}$ 혹은 $BRAF^{V600E}$ 유전자를 형질 도입시켜 만든 Nthy/$BRAF^{WT}$ (Nthy/WT)과 Nthy/$BRAF^{V600E}$ (Nthy/V600E) 세포주를 이종 이식하였다.

방법: Nthy/WT과 Nthy/V600E는 NSG 마우스의 피하에 주입되었다. 병리학적 분석을 위해 Hematoxylin & Eosin (H&E) 염색과 면역조직화학염색법을 수행하였다. $BRAF^{V600E}$ 선택적 억제제인 vemurafenib의 복강 투여를 통해 $BRAF^{V600E}$에 의한 종양형성 및 전이 능력 변화를 확인하였다. RNA 서열 분석 (RNA-sequencing)을 통해 세포주 내 전사체의 발현 변화를 확인하였고, 다른 암세포 유래 세포주 및 암조직들과의 전사체 발현 양상을 비교분석 하기 위해 미국 Broad Institute의 암

세포주백과사전 (CCLE)의 갑상선암 세포주 데이터와 유전자 발현 옴니버스 (GEO)의 GSE33630 암 조직 데이터를 활용하였다.

결과: Nthy/WT의 경우 6주 동안 체내 종양형성 및 전이 능력 모두 보이지 않은 반면, Nthy/V600E는 4주 동안 2784.343 mm^3 ± 922.463 mm^3 (평균 ± 표준편차, n = 11)에 도달하는 종양을 형성하며 약 72.7% (8/11)에서 주변 림프절 전이, 6-7주간 관찰 시 폐와 간으로의 전이가 확인되었다. Vemurafenib 투약은 통계적으로 유의한 종양성장속도 및 림프절 전이 억제 효과를 보였지만 종양의 세포사멸은 유도할 수 없었다. 병리 분석 결과, Nthy/V600E는 역분화갑상선암과 상당히 일치함을 보였다. 전사체 비교분석을 통해 Nthy/WT과 Nthy/V600E 사이에 5512개의 차별발현유전자 (|발현차| ≥ 2배, adjusted $p < 0.01$]가 존재함을 확인하고, 갑상선유두암과 정상 조직 간의 차별발현유전자보다 미분화갑상선암과 정상 조직 간의 차별발현유전자들과 더 유사함을 확인하였다. 또한, 분화와 암 예후와 연관된 유전자들의 발현 양상이 인간 미분화갑상선암 세포주인 8305c와 매우 유사함을 확인하였다. $BRAF^{V600E}$는 접촉 저지된 상태의 Nthy 세포주의 G1기 진행 관련 유전자는 증가시키고 G1/S기 정지 관련 유전자는 감소시켜 세포 주기를 활성화시켰다.

결론: 본 연구결과는 $BRAF^{V600E}$가 인간 정상 갑상선 세포의 암 발생에 중심적인 역할을 수행하며 SV40가 해당 세포주의 미분화갑상선암화 과정에 기여했을 가능성이 있음을 시사한다. 해당 세포주 이종이식모델은 미분화갑상선암의 원인병리론과 잠재적 치료 방안을 연구하기 위한 새로운 모델이 될 수 있을 것이다.

주요어: 갑상선 암화, $BRAF^{V600E}$ 돌연변이, 시미안 바이러스 40, 미분화 갑상선암, RNA-sequencing, 마우스 이종이식 모델, vemurafenib

학 번: 2017-22690